Available online at www.sciencedirect.com
ScienceDirect
Proceedings of the Combustion Institute 33 (2011) 1365–1371
Proceedings of the Combustion Institute
www.elsevier.com/locate/proci

LES of a laboratory-scale turbulent premixed Bunsen flame using FSD, PCM-FPI and thickened flame models

F.E. Hernández-Pérez *, F.T.C. Yuen, C.P.T. Groth, Ö.L. Gülder

Institute for Aerospace Studies, University of Toronto, 4925 Dufferin Street, Toronto, ON, Canada M3H 5T6

Available online 9 August 2010

Abstract

Large-eddy simulations (LES) of a turbulent premixed Bunsen flame were carried out with three subfilter-scale (SFS) modelling approaches for turbulent premixed combustion. One approach is based on the artificially thickened flame and power-law flame wrinkling models, the second approach is based on the presumed conditional moment (PCM) with flame prolongation of intrinsic low-dimensional manifolds (FPI) tabulated chemistry, and the third approach is based on a transport equation for the flame surface density (FSD). A lean methane–air flame at equivalence ratio $\phi = 0.7$, which was studied experimentally by Yuen and Gülder, was considered. The predicted LES solutions were compared to the experimental data. The resolved instantaneous three-dimensional structure of the predicted flames compares well with that of the experiment. Flame heights and resolvable flame surface density and curvature were also examined. In general, the average flame height was well predicted. Furthermore, the flame surface data extracted from the simulations showed remarkably good qualitative agreement with the experimental results. The probability density functions of predicted flame curvature displayed a Gaussian-like shape centred around zero as also observed in the experimental flame, although the experimental data showed a slightly wider profile. The results of the comparisons highlight the weaknesses and the strengths of SFS modelling approaches commonly used in LES of turbulent premixed flames.

Keywords: Turbulent premixed combustion; Large-eddy simulation; Thickened flame; FSD; PCM-FPI

1. Introduction

Large-eddy simulation (LES) is emerging as a promising computational tool for turbulent combustion processes [1]. However, a considerable complication for LES of turbulent premixed combustion is that chemical reactions occur in a thin reacting layer at extremely small-scales that cannot be resolved on LES grids and subfilter-scale (SFS) modelling of unresolved scales is required. In this study, three LES SFS modelling approaches for premixed turbulent combustion are compared and applied to a turbulent Bunsen flame. One approach is based on the artificially thickened flame [2] and power-law [3] flame wrinkling models, the second approach is based on the presumed conditional moment (PCM) [4] with flame prolongation of intrinsic low-dimensional manifolds (FPI) [5] tabulated chemistry, and the third approach is based on a transport equation for the flame surface density (FSD) [6]. Although a comparative study

* Corresponding author.
E-mail address: hperez@utias.utoronto.ca (F.E. Hernández-Pérez),

1540-7489/$ - see front matter © 2010 The Combustion Institute. Published by Elsevier Inc. All rights reserved.
doi:10.1016/j.proci.2010.06.010

of Bunsen flames was performed recently in which LES predictions obtained using a modified thickened flame model were compared with experimental data and other Reynolds-Averaged Navier–Stokes (RANS) solutions [7], there have been in general few head-to-head comparative studies of SFS and LES modelling approaches. Such studies are needed to advance LES for premixed combustion and clearly identify the predictive capabilities and limitations of SFS modelling. A lean methane–air flame at equivalence ratio $\phi = 0.7$, which has been studied experimentally by Yuen and Gülder [8], is considered. The capabilities of each SFS model to predict observed behaviour are examined and compared.

2. Favre-filtered governing equations

LES is based on a separation of scales, which is achieved via a low-pass filtering procedure. Scales larger than the filter size, Δ, are resolved, whereas scales smaller than Δ are modelled. Accordingly, a relevant flow parameter, φ, is filtered or Favre-filtered (mass-weighted filtering) to yield $\bar{\varphi}$ or $\bar{\varphi}$, respectively. The Favre-filtered form of the Navier–Stokes equations governing compressible flows of a thermally perfect reactive mixture of gases, neglecting Dufour, Soret and radiation effects, is used herein to describe turbulent premixed combustion processes. The equations are given by

$$\frac{\partial(\bar{\rho})}{\partial t} + \frac{\partial(\bar{\rho}\tilde{u}_i)}{\partial x_i} = 0\,, \tag{1}$$

$$\frac{\partial(\bar{\rho}\tilde{u}_i)}{\partial t} + \frac{\partial}{\partial x_j}\left(\bar{\rho}\tilde{u}_i\tilde{u}_j + \delta_{ij}\bar{p} - \check{\tau}_{ij}\right) = \bar{\rho}g_i + A_1\,, \tag{2}$$

$$\frac{\partial(\bar{\rho}\widetilde{E})}{\partial t} + \frac{\partial}{\partial x_i}\left[(\bar{\rho}\widetilde{E} + \bar{p})\tilde{u}_i + \check{q}_i\right] - \frac{\partial}{\partial x_j}\left(\check{\tau}_{ij}\tilde{u}_i\right) = \bar{\rho}g_i\tilde{u}_i + B_1 + B_2 + B_3\,, \tag{3}$$

$$\frac{\partial(\bar{\rho}\widetilde{Y}_k)}{\partial t} + \frac{\partial(\bar{\rho}\widetilde{Y}_k\tilde{u}_i)}{\partial x_i} + \frac{\partial \check{\mathscr{J}}_{k,i}}{\partial x_i} = \overline{\dot{\omega}}_k + C_1\,, \tag{4}$$

where $\bar{\rho}$ is the filtered mixture density, $\tilde{u}_i$ is the Favre-filtered mixture velocity, $\bar{p}$ is the filtered mixture pressure, $\widetilde{Y}_k$ is the Favre-filtered mass fraction of species k, $\widetilde{E}$ is the Favre-filtered total mixture energy (including chemical energy) given by $\widetilde{E} = \sum_{k=1}^{N}\widetilde{Y}_k(\check{h}_k + \Delta h^0_{f,k}) - \bar{p}/\bar{\rho} + \widetilde{u_i u_i}/2; \check{h}_k, \Delta h^0_{f,k}$ and $\overline{\dot{\omega}}_k$ are the sensible enthalpy, heat of formation and the filtered reaction rate of species k, respectively, and g_i is the acceleration due to gravity. The filtered equation of state has the form $\bar{p} = \bar{\rho}R\widetilde{T}$. The resolved stress tensor, $\check{\tau}_{ij}$, the resolved total heat flux, $\check{q}_i$, and the resolved species diffusive fluxes, $\check{\mathscr{J}}_{k,i}$, are evaluated in terms of the filtered quantities.

The terms, A_1, B_1, B_2, B_3, and C_1, arise from the low-pass filtering process and require modelling. These terms are expressed as $A_1 = -\frac{\partial[\bar{\rho}(\widetilde{u_i u_j} - \tilde{u}_i\tilde{u}_j)]}{\partial x_j}$, $B_1 = -\frac{\partial[\bar{\rho}(\widetilde{hu_i} - \check{h}\tilde{u}_i)]}{\partial x_i}$, $B_2 = -\frac{1}{2}\frac{\partial[\bar{\rho}(\widetilde{u_j u_j u_i} - \tilde{u}_j\tilde{u}_j\tilde{u}_i)]}{\partial x_i}$, $C_1 = -\frac{\partial[\bar{\rho}(\widetilde{Y_k u_i} - \widetilde{Y}_k\tilde{u}_i)]}{\partial x_i}$, $B_3 = -\frac{\partial\left[\sum_{k=1}^{N}\Delta h^0_{f,k}\bar{\rho}(\widetilde{Y_k u_i} - \widetilde{Y}_k\tilde{u}_i)\right]}{\partial x_i}$, and must be modelled for closure of the filtered equation set. The subfilter stresses, $\sigma_{ij} = -\bar{\rho}\,(\widetilde{u_i u_j} - \tilde{u}_i\tilde{u}_j)$, are modelled using an eddy-viscosity type model with $\sigma_{ij} = 2\bar{\rho}\nu_t(\check{S}_{ij} - \delta_{ij}\check{S}_{ll}/3) + \delta_{ij}\,\sigma_{ll}/3$. The SFS turbulent viscosity, ν_t, is prescribed herein by using a one-equation model [9] for the SFS turbulent kinetic energy, $\tilde{k}_\Delta$. Standard gradient-based approximations are used in this work for the modelling of the SFS fluxes B_1, B_3, and C_1. The subfilter turbulent diffusion term, B_2, is modelled as suggested by Knight et al. [10] with $-\bar{\rho}(\widetilde{u_i u_i u_j} - \tilde{u}_i\tilde{u}_i\tilde{u}_j)/2 = \sigma_{ij}\tilde{u}_i$.

3. Thickened flame model

One approach to modelling the turbulence/chemistry interaction for premixed flames is offered by the so-called thickened flame model. In the thickened flame model, the computed flame front structure is artificially locally thickened by a factor, F, in such a way that it can be resolved on a relatively coarse LES mesh, but such that the flame speed remains unaltered [2]. An efficiency factor, E_F, is also introduced to account for the resulting decrease in the flame Damkhöler number, Da [2]. The resulting filtered balance equation for chemical species takes the modified form

$$\frac{\partial(\bar{\rho}\widetilde{Y}_k)}{\partial t} + \frac{\partial(\bar{\rho}\widetilde{Y}_k\tilde{u}_i)}{\partial x_i} = \frac{\partial}{\partial x_i}\left(E_F F\bar{\rho}\mathscr{D}_k\frac{\partial\widetilde{Y}_k}{\partial x_i}\right) + \frac{E_F\overline{\dot{\omega}}_k}{F}, \tag{5}$$

where the filtered reaction rates, $\overline{\dot{\omega}}_k$, are now computed directly by using Arrhenius law reaction rates evaluated in terms of resolved quantities.

The efficiency factor, E_F, is evaluated using a power-law flame wrinkling model that assumes that the internal structure of the flame is not significantly altered by turbulence. The power-law expression is given by [3]

$$\Xi_{\Delta_o} = \left[1 + \min\left(\frac{\Delta_o}{\delta_L}, \Gamma_{\Delta_o}\frac{u'_{\Delta_o}}{s_L}\right)\right]^{\gamma} = E_F, \tag{6}$$

where Ξ_{Δ_o} is the SFS wrinkling factor, Δ_o is the outer cutoff scale, and γ is the power of the expression, which is taken to be 0.5 here [3]. The inner cutoff is associated with the maximum of the laminar flame thickness, δ_L, and the inverse of the mean curvature of the flame, which can be estimated by assuming equilibrium between production

and destruction of flame surface density as $|\langle \nabla \cdot \mathbf{n} \rangle| = \Delta_o^{-1}(u'_{\Delta_o}/s_L)\Gamma_{\Delta_o}$, where $\mathbf{n}$ is a unit vector normal to the flame surface, Γ_{Δ_o} is the efficiency function proposed by Charlette et al. [3] to account for the net straining of all relevant scales smaller than Δ_o and s_L is the laminar flame speed. The SFS rms velocity u'_{Δ_o}, is calculated using the expression proposed by Colin et al. [2].

4. Flame surface density model

Another approach to modelling of turbulent premixed flames is to ignore for the most part the internal structure of the flame and detailed chemical kinetics, and represent the combustion occurring at the flame front in terms of a reaction progress variable. The modelled progress variable equation has the form

$$\frac{\partial(\bar{\rho}\tilde{c})}{\partial t} + \frac{\partial(\bar{\rho}\tilde{c}\tilde{u}_i)}{\partial x_i} = \frac{\partial}{\partial x_i}\left(\frac{\bar{\rho}\nu_t}{Sc_t}\frac{\partial \tilde{c}}{\partial x_i}\right) + \rho_r s_L \bar{\rho}\widetilde{\Sigma}, \qquad (7)$$

where ρ_r is the reactants density, $\widetilde{\Sigma}$ is the Favre-filtered flame surface area per unit mass of the mixture, and the product, $\bar{\rho}\widetilde{\Sigma}$, is the flame surface area per unit volume or flame surface density (FSD).

The filtered quantity, $\widetilde{\Sigma}$, includes contributions from the resolved FSD and the unresolved subfilter-scales. The latter must be modelled. A modelled transport equation for the FSD density has been proposed by Hawkes and Cant [6] and is given by

$$\begin{aligned}\frac{\partial(\bar{\rho}\widetilde{\Sigma})}{\partial t} &+ \frac{\partial(\bar{\rho}\tilde{u}_i\widetilde{\Sigma})}{\partial x_i} - \frac{\partial}{\partial x_i}\left(\frac{\bar{\rho}\nu_t}{Sc_t}\frac{\partial\widetilde{\Sigma}}{\partial x_i}\right)\\ &= \Gamma_K\bar{\rho}\widetilde{\Sigma}\frac{\sqrt{\tilde{k}_\Delta}}{\Delta} - \beta s_L\frac{(\bar{\rho}\widetilde{\Sigma})^2}{1-\tilde{c}}\\ &\quad + (\delta_{ij} - n_{ij})\bar{\rho}\widetilde{\Sigma}\frac{\partial\tilde{u}_i}{\partial x_j} - \frac{\partial}{\partial x_i}[s_L(1+\tau\tilde{c})M_i\bar{\rho}\widetilde{\Sigma}]\\ &\quad + s_L(1+\tau\tilde{c})\bar{\rho}\widetilde{\Sigma}\frac{\partial M_i}{\partial x_i}, \end{aligned} \qquad (8)$$

where $\vec{M} = -\nabla\bar{c}/\widetilde{\Sigma}$ is the flamelet model for the surface averaged normal ($\bar{c}$ is estimated using $\bar{c} = (1+\tau)\tilde{c}/(1+\tau\tilde{c})$), $\alpha = 1 - \vec{M}\cdot\vec{M}$, and $n_{ij} = M_iM_j + 1/3\alpha\delta_{ij}$. The variable $\tau = (T_{ad} - T_r)/T_r$ is the heat release parameter, where T_{ad} and T_r are the adiabatic and the reactants temperature, respectively, β is a model constant and must satisfy $\beta \geqslant 1$ for realisability requirements, α is a resolution factor, and Γ_K is an efficiency function [11]. The terms on the left hand side of the modelled FSD equation represent unsteady, convection and SFS transport effects, while the terms on the right hand side represent the production/destruction sources associated with SFS strain and curvature, resolved strain, resolved propagation and curvature.

5. PCM-FPI

The presumed conditional moment-FPI (PCM-FPI) [4] is an approach that combines presumed probability density functions (PDF) and chemistry tabulated from prototype combustion problems using flame prolongation of ILDM (FPI) [5]. When turbulent premixed combustion is considered, look-up tables of filtered terms associated with chemistry are built from laminar premixed flamelets.

The main objective of the FPI tabulation technique is to reduce the cost of performing reactive flow computations with large chemical kinetic mechanisms by building databases of relevant quantities based on detailed simulations of simple flames. Relevant chemical parameters such as species mass fractions or reaction rates are then related to a single progress of reaction variable, Y_c. For instance, any property φ_j (species mass fractions or reaction rates) of a steady-state laminar premixed flame at equivalence ratio ϕ_0 may be expressed as a function of position normal to the flame front, x, as $\varphi_j = \varphi_j(\phi_0, x)$, which can then be mapped to the progress variable space, Y_c, eliminating x. The resulting FPI table may then be written: $\varphi_j^{FPI}(\phi_0, Y_c) = \varphi_j(\phi_0, x)$. Previous studies by Fiorina et al. [12] have shown that for methane–air combustion an appropriate choice for the progress of reaction is $Y_c = Y_{CO_2} + Y_{CO}$.

In the context of LES of turbulent premixed flames, a filtered quantity can be obtained via

$$\tilde{\varphi}_j = \int_0^1 \varphi_j^{FPI}\widetilde{P}(c^*)\,dc^*, \qquad (9)$$

where c is the progress variable and $\widetilde{P}(c^*)$ is the filtered probability density function of c, which needs to be determined. The PDF of c is taken to be a beta-distribution [13,14] and can be constructed from the resolved progress variable, $\tilde{c}$, and its SFS variance, $c_v = \widetilde{cc} - \tilde{c}\tilde{c}$. These two variables, $\tilde{c}$ and c_v, are linked to the progress of reaction $\widetilde{Y}_c$ and its SFS variance, Y_{c_v}. The filtered progress variable is defined as the filtered progress of reaction normalized by its value at equilibrium: $\tilde{c} = \widetilde{Y}_c/Y_c^{Eq}(\phi_0)$. The variance of c may be obtained from $\widetilde{Y}_c, Y_c^{Eq}(\phi_0)$ and the variance of the progress of reaction, $Y_{c_v} = \widetilde{Y_cY_c} - \widetilde{Y}_c\widetilde{Y}_c$. The expression for c_v is $c_v = Y_{c_v}/Y_c^{Eq^2}(\phi_0)$. Modelled balance equations are used to determine Y_c and Y_{c_v} [4,13,14]. The modelled transport equation for $\widetilde{Y}_c$ has the form

$$\frac{\partial(\bar{\rho}\widetilde{Y}_c)}{\partial t} + \frac{\partial(\bar{\rho}\tilde{u}_i\widetilde{Y}_c)}{\partial x_i} = \frac{\partial}{\partial x_i}\left[\bar{\rho}(\breve{\mathscr{D}}_{Y_c} + \mathscr{D}_t)\frac{\partial\widetilde{Y}_c}{\partial x_i}\right] + \overline{\dot{\omega}}_{Y_c}, \qquad (10)$$

where $\overline{\dot{\omega}}_{Y_c}$ is a source term due to chemistry, $\breve{\mathscr{D}}_{Y_c}$ is the diffusion coefficient associated with Y_c, and $\mathscr{D}_t$

is the turbulent diffusion coefficient used to model SFS scalar transport. A similar balance equation for Y_{c_v} is used. It is important to remark that a reaction rate can be written as $\dot{\omega} = \rho\dot{\omega}^*$, therefore $\overline{\dot{\omega}} = \bar{\rho}\tilde{\dot{\omega}}^*$ and $\overline{Y_c\dot{\omega}_{Y_c}} = \bar{\rho}\widetilde{Y_c\dot{\omega}^*_{Y_c}}$. The latter is a reaction rate term appearing in the transport equation for Y_{c_v}. The terms $\tilde{\dot{\omega}}^*_{Y_c}$ and $\widetilde{Y_c\dot{\omega}^*_{Y_c}}$ are included in the tabulated database. By introducing the segregation factor, $S_c = c_v/(\tilde{c}(1-\tilde{c}))$, a look-up table of filtered quantities $\tilde{\varphi}_j^{PCM}(\phi_0, \tilde{c}, S_c)$, can be pre-generated for use in subsequent LES calculations.

6. Burner setup

Yuen and Gülder [8] considered an axisymmetric Bunsen-type burner with an inner nozzle diameter of 11.2 mm to generate premixed turbulent conical flames stabilized by annular pilot flames. Flame front images were captured using planar Rayleigh scattering achieving a resolution of 45 μm/pixel. The Rayleigh scattering images were converted into temperature field and further processed to provide the temperature gradient and two-dimensional curvature. Particle image velocimetry was used to measure the instantaneous velocity field for the experimental conditions.

The flame considered in this work corresponds to a lean premixed methane–air flame at an equivalence ratio of $\phi = 0.7$ and atmospheric pressure. The turbulence at the burner exit was characterized by a non-dimensional turbulence intensity $u'/s_L = 14.38$ and an integral length scale $L_t = 1.79$ mm. The mixture of reactants was at a temperature of 300 K and its mean velocity was 15.6 m/s. The flame lies in the thickened wrinkled flame or thin reaction zone of the turbulent premixed combustion diagram and the corresponding turbulent Reynolds number is 324.

In the simulations, a cylindrical domain having a diameter of 0.05 m and a height of 0.1 m was employed and discretized with a grid consisting of 1,638,400 hexahedral cells. The pilot flame was approximated by a uniform inflow of hot combustion products at a velocity of 16.81 m/s. For the burner exit, a uniform mean inflow of reactants with superimposed turbulent fluctuations was prescribed. The velocity fluctuations were pre-generated using the procedure developed by Rogallo [15] and superimposed onto the mean inflow velocity using Taylor's hypothesis of frozen turbulence. The same velocity fluctuations were used for all the simulations.

For the numerical results presented herein, thermodynamic and molecular transport properties of each mixture component are prescribed using the database compiled by Gordon and McBride [16,17]. In the thickened flame simulation, methane–air chemistry was represented by a one-step reaction mechanism as described by Westbrook and Dryer [18] and a constant thickening factor $F = 3$ was utilized. Two different simulations with the PCM-FPI model were run. In one case, species mass fractions were directly obtained from the look-up table. In the other one, the transport equations for species were solved, reconstructing the reaction rates based on a high Damköler number approximation described in Refs. [13,14]. The chemistry look-up table for the PCM-FPI simulations was generated from the steady-state solution of a one-dimensional laminar premixed flame obtained with the Cantera package [19] for a methane–air flame with the GRI-Mech 3.0 mechanism [20]. A reduced number of 10 species were selected and tabulated based on their contributions to mixture mass and energy [14]. The species are: CH_4, O_2, N_2, H_2O, CO_2, CO, H_2, H, OH and C_2H_2. The tabulated species mass fractions and the terms $\tilde{\dot{\omega}}^*_{Y_c}$ and $\widetilde{Y_c\dot{\omega}^*_{Y_c}}$ were retrieved from the look-up table, which had 145 values of $\tilde{c}$ and 25 values of S_c.

The Favre-filtered transport equations described above are solved on multi-block hexahedral meshes employing a second-order accurate parallel finite-volume scheme [21]. The inviscid flux at each cell face is evaluated using limited linear reconstruction [22] and Riemann-solver based flux functions [23,24], while the viscous flux is evaluated utilizing a hybrid average gradient-diamond path method [25]. A explicit second-order Runge–Kutta scheme was used to time-march the solutions. Parallel implementation of the finite-volume scheme has been carried out via domain decomposition using the C++ programming language and the MPI (message passing interface) library.

7. Results and discussion

In what follows, the numerical solutions obtained with the different models are identified as PCM-FPI, PCM-FPI-RR, TF3 and C-FSD results. The difference between the PCM-FPI and PCM-FPI-RR is that the species mass fractions were transported and their reaction rates were reconstructed for PCM-FPI-RR, whereas species mass fraction were directly read from the look-up table for PCM-FPI.

7.1. Instantaneous flame front

Three-dimensional views of the predicted instantaneous flame surface, identified by the isotherm $\tilde{T} = 1076$ K, are displayed in Fig. 1 corresponding to time $t = 4$ ms after the initiation of the simulation, for which a quasi-steady flame structure has been achieved in each case. The simulated flames exhibit a highly wrinkled surface and the scale of wrinkling becomes larger near the tips of the flames. Moreover, the overall predicted flame structure is quite similar for each of the SFS models, although the FSD model results

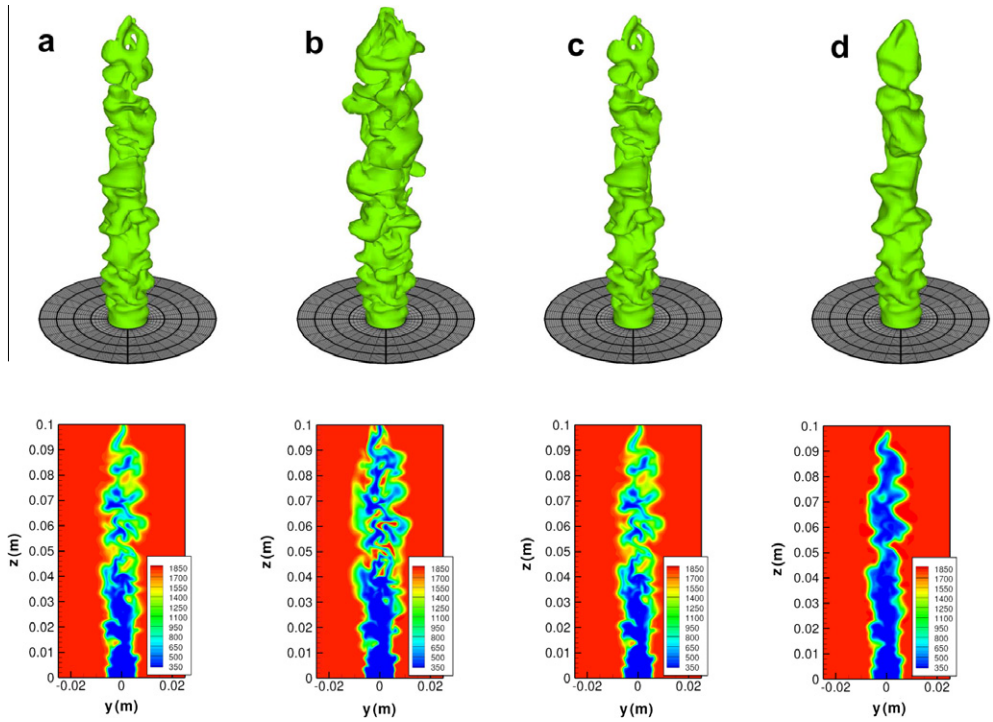

Fig. 1. Instantaneous flame iso-surface $\widetilde{T} = 1076$ K at 4 ms after the initiation of the simulations. (a) PCM-FPI, (b) C-FSD, (c) PCM-FPI-RR, (d) TF3.

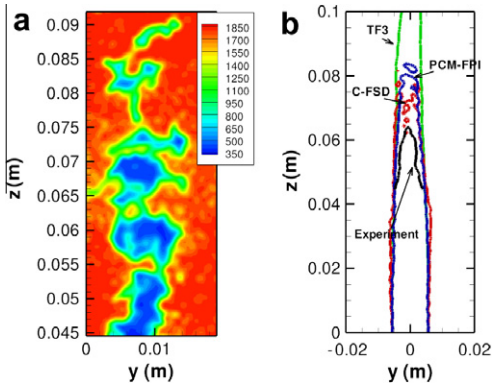

Fig. 2. Instantaneous filtered temperature from the experiment and 0.5 contour of the averaged c_T map from the experiment and the simulations. (a) Filtered image, (b) $\langle c_T \rangle = 0.5$.

would seem to exhibit the most wrinkling and the thickened flame shows considerably less resolved wrinkling than its counterparts.

In the C-FSD case of Fig. 1b, a more spread flame is observed. The PCM-FPI (Fig. 1a) and PCM-FPI-RR (Fig. 1c) solutions display a nearly identical structure, whereas the artificially thickened flame (Fig. 1d) is considerably less wrinkled than those of the other models. This observation can be attributed to the fact that turbulent structures smaller than the flame front thickness are unable to wrinkle the thickened flame front.

More details of the internal structure of the flames can be seen in the lower part of Fig. 1, where planar cuts of the four instantaneous solutions are shown. The solutions are in close agreement with each other up to nearly 3 cm above the bottom line. Further downstream, particularly in the region above 5 cm of the burner exit, clear differences are noticeable. Pockets of unburned reactants can be identified in Fig. 1a–c, which are not present in Fig. 1d. For direct comparison, a filtered instantaneous image of the experimental flame is shown in Fig. 2a obtained with a filter-width equal to that of the computations. As it can be seen, the numerical simulations are able to reproduce, at least qualitatively, key features of the experimental flame front.

7.2. Flame surface density

To extract the flame surface density from the experimental data, the Rayleigh scattering images were processed to obtain progress variable fields based on temperature. This progress variable is defined as $c_T = (T - T_u)/(T_b - T_u)$, where T is the local temperature, T_u is the unburnt gas temperature and T_b is the fully burnt gas temperature. The two-dimensional (2D) maps of the FSD were

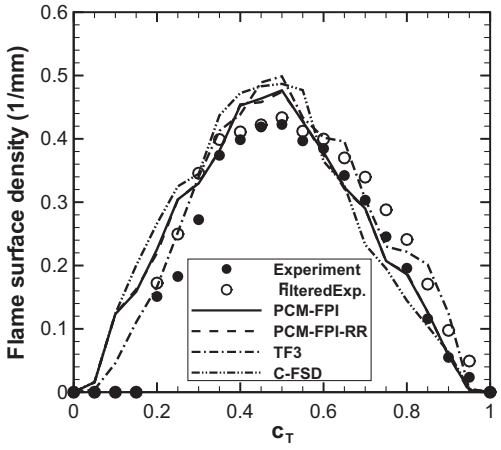

Fig. 3. 2D flame surface density extracted from the experimental data and LES simulations.

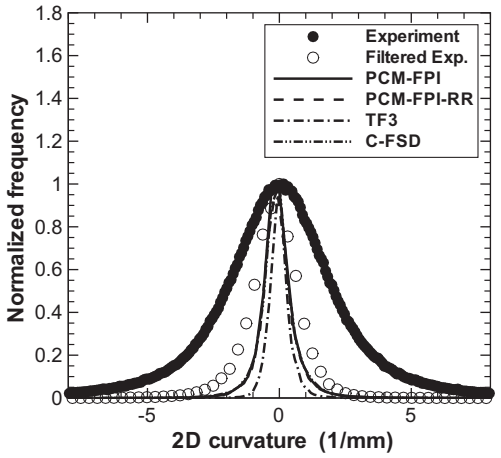

Fig. 4. PDF of 2D curvature corresponding to a progress variable $c_T = 0.5$.

computed by using the method developed by Shepherd [26], in which instantaneous flame front edges are superimposed onto the averaged c_T map to calculate the length over area ratio for a given c_T. The same procedure was then applied to 2D slices of the resolved temperature field obtained from the LES simulations. Since LES provides solutions of filtered variables, it is more appropriate to compare the numerical results with filtered experimental data. The experimental temperature images were therefore first filtered with a top-hat filter having a characteristic size of two times the average cell size of the LES computational grid. The total number of post-processed experimental images was 300 and, for each LES simulation, the 2D slices were extracted from 19 instantaneous snapshots of the numerical solution separated by 0.25 ms.

Predictions of the average map of $c_T = 0.5$ for the three SFS models are compared with the map obtained from the Rayleigh scattering images in Fig. 2b. Although it is quite evident that the thickened flame model over-predicts the average flame height by a considerable margin, both C-FSD and PCM-FPI models yield flame heights (7 cm and 7.75 cm, respectively) that agree very well with the experimental value, which is estimated to be about 6.5 cm based on the $c_T = 0.5$ contour.

The 2D FSD values extracted from the simulations and the experiment are compared in Fig. 3. It can be seen that all the FSD profiles obtained from the simulations qualitatively reproduce the trends observed in the experimental data. In all the profiles the maximum FSD value is found around $c_T = 0.5$. The peak FSD values obtained from the simulations are higher than the experimental ones. Despite quantitative discrepancies observed, 2D FSD profiles obtained from the simulations show very good qualitative agreement with the experimental FSD profiles.

7.3. Flame front curvature

Two-dimensional curvature was also extracted from instantaneous experimental images and slices of the numerical solutions. The curvature PDFs of the experimental data, filtered experimental data and the different LES solutions, corresponding to $c_T = 0.5$ are shown in Fig. 4. The PDFs display a Gaussian-type shape centred around zero. It can be highlighted that filtering the experimental data leads to a narrower PDF, which is due to the fact that filtering removes small-scale wrinkled structures having larger curvatures. All the LES solutions exhibit a narrow PDF as compared to the experimental ones. It can also be seen that the PDFs obtained from the C-FSD, PCM-FPI and PCM-FPI-RR simulations nearly overlap with each other and the filtered experimental results, whereas the PDF obtained from the TF3 simulation is the most narrow. These trends indicate that more small-scale wrinkling is captured by the C-FSD and PCM-FPI models, as compared to the thickened flame model.

8. Concluding remarks

The present comparison of SFS model results for LES of a turbulent lean premixed methane–air Bunsen flame to the experimental results of Yuen and Gülder [8] has revealed a number of deficiencies in the thickened flame model, even with a relatively small value of 3 for the thickening factor. The flame height was significantly over-predicted, the instantaneous flame front exhibits noticeably less wrinkling

than the actual experimental flame, and the resolved curvature of the flame front is under-predicted. These deficiencies would be even more pronounced if a large thickening factor were adopted as is more typically used.

In contrast, the performance of the C-FSD, PCM-FPI, and PCM-FPI-RR models was found to be much better, with all three approaches providing predictions that agree both qualitatively and quantitatively with key aspects of the flame observed in the experiment. The resolved flame structure and wrinkling, average flame height, and resolved flame surface and curvature all compare well with experiment. The FSD model appears to be best suited for describing the evolution and dynamics of the flame surface, yielding slightly better predictions of these quantities, but is lacking in terms its connection of flame area to reaction rates. The PCM-FPI model seems more rubust and can be applied more widely to premixed, non-premixed, and partially premixed flames, although at the expense of higher computational costs (computational costs of the LES with the PCM-FPI-RR SFS model were about 55% more than those of the C-FSD model). Future research will involve further comparisons of the SFS models for the premixed flame considered here at other turbulence intensities and to compare predictions of turbulent burning rate to experimental estimates of those values.

Acknowledgements

Computational resources for performing all of the calculations reported herein were provided by the SciNet High Performance Computing Consortium at the University of Toronto and Compute/Calcul Canada through funding from the Canada Foundation for Innovation (CFI) and the Province of Ontario, Canada. The first author gratefully acknowledges the support received from the Mexican National Council for Science and Technology (CONACYT) and the European Community's Sixth Framework Programme (Marie Curie Early Stage Research Training Fellowship) under contract number MEST-CT-2005-020426.

References

[1] H. Pitsch, *Annu. Rev. Fluid Mech.* 38 (2006) 453–482.
[2] O. Colin, F. Ducros, D. Veynante, T. Poinsot, *Phys. Fluids* 12 (2000) 1843–1863.
[3] F. Charlette, C. Meneveau, D. Veynante, *Combust. Flame* 131 (2002) 159–180.
[4] P. Domingo, L. Vervisch, S. Payet, R. Hauguel, *Combust. Flame* 143 (2005) 566–586.
[5] O. Gicquel, N. Darabiha, D. Thévenin, *Proc. Combust. Inst.* 28 (2000) 1901–1908.
[6] E.R. Hawkes, R.S. Cant, *Combust. Flame* 126 (2001) 1617–1629.
[7] A. De, S. Acharya, *Combust. Sci. Tech.* 181 (2009) 1231–1272.
[8] F.T.C. Yuen, O.L. Gülder, *Proc. Combust. Inst.* 32 (2009) 1747–1754.
[9] A. Yoshizawa, K. Horiuti, *J. Phys. Soc. Jpn.* 54 (1985) 2834–2839.
[10] D. Knight, G. Zhou, N. Okong'o, V. Shukla, Paper 98-0535, AIAA, January 1998.
[11] C. Meneveau, T. Poinsot, *Combust. Flame* 86 (1991) 311–332.
[12] B. Fiorina, O. Gicquel, L. Vervisch, S. Carpentier, N. Darabiha, *Proc. Combust. Inst.* 30 (2005) 867–874.
[13] P. Domingo, L. Vervisch, D. Veynante, *Combust. Flame* 152 (2008) 415–432.
[14] J. Galpin, A. Naudin, L. Vervisch, C. Angelberger, O. Colin, P. Domingo, *Combust. Flame* 155 (2008) 247–266.
[15] R.S. Rogallo, *NASA Tech. Memo.* 81315 (1981).
[16] S. Gordon, B.J. McBride, *NASA Ref. Pub.* 1311 (1994).
[17] B.J. McBride, S. Gordon, *NASA Ref. Pub.* 1311 (1996).
[18] C.K. Westbrook, F.L. Dryer, *Combust. Sci. Tech.* 27 (1981) 31–43.
[19] D. Goodwin, H.K. Moffat, Cantera, available at <http://code.google.com/p/cantera/>.
[20] G.P. Smith, D.M. Golden, M. Frenklach, N.W. Moriarty, B. Eiteneer, M. Goldenberg et al., GRI-Mech 3.0, available at <http://www.me.berkeley.edu/gri_mech/>.
[21] X. Gao, C.P.T. Groth, *J. Comput. Phys.* 229 (2010) 3250–3275.
[22] T.J. Barth, Paper 93-0668, AIAA, January 1993.
[23] P.L. Roe, *J. Comput. Phys.* 43 (1981) 357–372.
[24] M.-S. Liou, *J. Comput. Phys.* 214 (2006) 137–170.
[25] S.R. Mathur, J.Y. Murthy, *Numer. Heat Transfer* 31 (1997) 191–215.
[26] I. Shepherd, *Proc. Combust. Inst.* 26 (1996) 373–379.